Toward a Classification System for the Shape, Location, and Orientation of Hill-Sachs Lesions

Amanda Eskinazi

A Report Submitted to the Faculty of the

Graduate Interdisciplinary Program in
Biomedical Engineering

In Partial Fulfillment of the Requirements
For the Degree of

MASTER OF SCIENCE

With a Major in Biomedical Engineering
In the Graduate College

THE UNIVERSITY OF ARIZONA

May 11, 2011

Table of Contents

List of Figures

List of Tables

1. Abstract

A Hill-Sachs lesion (HSL) is a compression fracture on the humeral head created when the soft humeral head impacts the edge of the glenoid during shoulder dislocation. HSL incidence is reported in 47% of acute anterior glenohumeral dislocations and in 40-80% of patients with chronic instability. A Bankart lesion, the avulsion of the anterior/inferior labrum and inferior glenohumeral ligament from the glenoid rim, is often accompanied by a HSL. Soft tissue repairs are often unsuccessful when a significant bony defect is left untreated; it is our long-term goal to determine which bony defects should be treated to prevent failure of soft tissue repair. Surgeons have proposed the presence of "large" HSLs or the position and orientation of the HSL as causes for recurrent dislocation following Bankart repair. Unfortunately, in the orthopedic literature there is no system for classifying HSLs, or even for quantifying their size, position, and/or orientation which precludes the objective comparison of the work of various authors. The development of such a system is the necessary precursor to the production of any meaningful conclusions about the significance of the HSL. An inexpensive medical image segmentation process using active contours was implemented to build 3D reconstructions of the humeral head. Each of the active contour parameters was optimized for the clinical data set. Literature studies were conducted to come to a consensus on critical lesion traits and methods for computationally quantifying the lesion's traits. The long-term goal of this study is to compare clinical outcomes to the quantitative measures determined using this method.

2. Background

A Hill-Sachs lesion (HSL) is an impaction fracture on the humeral head, commonly associated with glenohumeral instability, created when the humeral head impacts the edge of the glenoid during shoulder dislocation. The basic anatomy of the shoulder is shown in **Figure 1**.

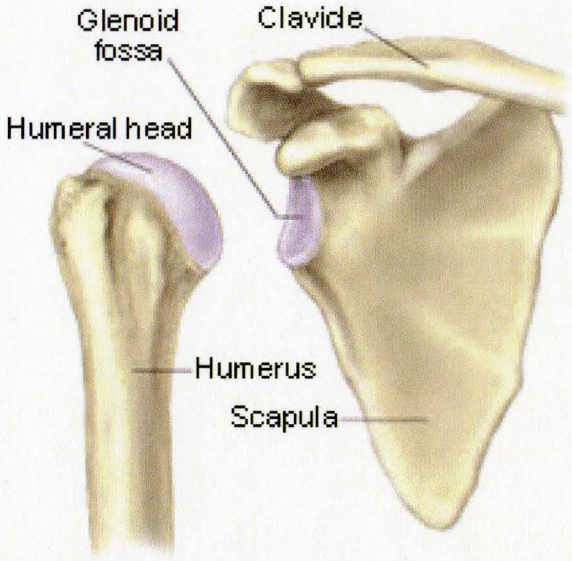

Figure 1. The shoulder is composed of three bones: the clavicle, the scapula, and the humerus. Hill-Sachs lesions are impaction fractures of the humeral head (www.shoulderandelbowcenter.com).

While a joint such as the hip's ball and socket provides stability with the femoral head largely contained within the acetabulum, the glenohumeral joint is uniquely the most mobile joint in the human body due to a surface area mismatch between the glenoid and the humerus. As a result, the shoulder is the most commonly dislocated joint in the body [1-3] with repeat dislocations being especially common among young [4] and active people. The limited interface between the glenoid fossa and the humeral head means that the shoulder joint relies heavily on surrounding structures and ligaments for stability. For example, the glenoid labrum is a layer of soft tissue that surrounds the rim of the glenoid fossa, deepening the socket and improving stability. Damage to the labrum and loss of glenoid bone, respectively known as Bankart and

bony Bankart lesions, seriously compromise the long-term stability of the joint. The presence of a HSL is believed to have an influence on glenohumeral stability following Bankart repair. HSL incidence is reported in 47-100% of first-time dislocations in young patients [5-8]. In a group of patients with recurrent dislocations, HSL prevalence was 75.8% [9].

In recent years, arthroscopic Bankart repair has become a common alternative to the more invasive open repair for patients with shoulder instability. While the minimally invasive nature of arthroscopic repair allows for speedier recovery, patients with bony defects are also more susceptible to requiring reintervention due to continued glenohumeral instability. In a study of 194 arthroscopic repairs, there was a 4% recurrence rate of dislocation in patients without significant bone defects (6.5% in contact athletes) versus a 67% recurrence rate in patients with significant bone loss (89% in contact athletes) [10]. While this data certainly implies that severity of bone loss is related to surgical outcome, prevalent across the literature is uncertainty as to what qualifies as "significant" bone loss.

In addition to HSL size, surgeons have proposed that other factors, including position and orientation of the lesion, may also play a role in the success rate of the arthroscopic procedure [10]. Unfortunately, in the orthopedic literature there is no system for classifying HSLs, or even quantifying their size, position, and/or orientation. The lack of such a system precludes the objective comparison of the work of various authors. The development of such a system is the necessary precursor to the production of any meaningful conclusions about the significance of the HSL. To work toward a solution, this study has been broadly divided into two parts: 1. preliminary categorization and methods for characterizing bone loss traits such as size, location, and orientation and 2. 3D reconstruction of the humeral head using HSL patient data.

3. Characterization of Hill-Sachs Lesion

3.1 Introduction

The anatomy of the Bankart and Hill-Sachs lesions are critical determinants of patient dislocation recurrence rate, surgical planning, and post-operative success. The Bankart lesion, for example, characterized by damage to the anterior-inferior glenoid labrum, has been shown to highly compromise glenohumeral stability if it was greater than 21% of the glenoid length [11, 12]. These measures were quantified physically and via medical image analysis, and consistently showed that such a defect resulted in 50% width loss across a single axial cross section of the inferior glenoid. Studies have also been done to characterize the shape of the glenoid to better understand the type and severity of the lesion. The glenoid is typically pear-shaped, meaning in a sagittal view the inferior region is wider than the superior region. Large bony Bankart lesions by nature compromise the width of the inferior region, often creating an inverted pear shape. The shape of the injured glenoid can vary due to the amount of bone loss. Patients are subject to a 61% dislocation rate with, compared to 4% without, an inverted pear glenoid [10, 13]. Finally, investigators concerned with glenoid injury have identified the glenoid bare spot, located at the geometric center of the inferior glenoid, as a reference point from which to accurately measure anatomy of the injury [13].

The quantitative and qualitative information gleaned from studying the Bankart lesion has allowed for strong trends to be established in patient treatment. Repair can be carried out traditionally or arthroscopically, both of which involve roughening the bone surface (to enhance ligament reattachment) and reattaching the capsule, labrum, and inferior glenohumeral ligament to the glenoid rim using suture anchors. This procedure is most effective if the damage does not extend beyond the glenoid labrum, the soft tissue surrounding the glenoid fossa. For large bony

lesions of the glenoid, a Latarjet procedure is carried out in which a portion of the coracoid, a bony outgrowth next to the joint is released and screwed on to the defect to fill it in. As is evident, these procedures vary greatly in their need and purpose. The orthopedic community has been able to identify factors that influence the decision making process for these procedures. It is that level of understanding that we hope to also achieve by studying the HSL.

The first characteristics we are interested in with respect to the HSL are shape and size. Shape is often discussed in terms of length, width, and depth while these traits, in addition to volume, can be used to characterize size. While many studies qualitatively group lesions into groups of different size, others have quantified lesions in cadaveric studies or during surgery. To aid surgeons pre-operatively, we should be able to determine the size of the lesion radiographically. Also, it is important to discuss which method of characterizing size most accurately predicts clinical outcomes.

In radiographic scans, the location of the lesion is typically at the level of the coracoid, definitely within the superior half of the humeral head. The lesion can also be characterized as being on the anterior or posterior side of the articular surface. Anteroposterior position is important to be aware of with each individual, who may be more prone to anterior or posterior dislocations. Since anterior dislocations are most common, one would be concerned with posterior lesions in this case. The opposite applies to anterior lesions should an individual experience recurrent posterior dislocations.

The orientation of the lesion can be designated either engaging or non-engaging. An engaging HSL is oriented such that when the arm is externally rotated the edge of the lesion drops over the glenoid rim as is shown on the right side of Figure 2. Non-engaging lesions do not align with the glenoid rim in a functional position.

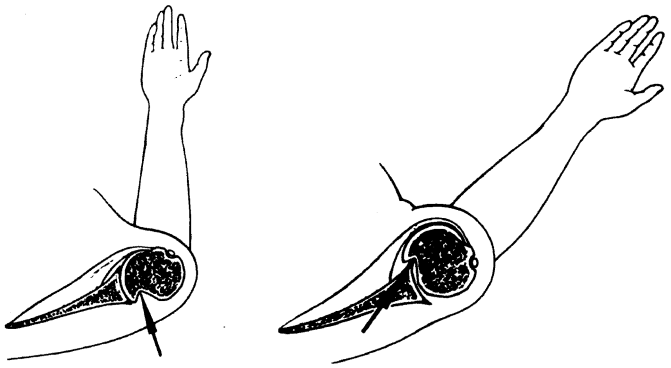

Figure 2. Drawings showing a posterior-superior impression fracture of the humeral head, with the arm in neutral rotation (left) and external rotation (right). In external rotation the lesions slips over the anterior rim of the glenoid. [14]

In designing a classification system for HSLs, it is important to understand how the characteristics of the lesion drive surgical procedure decisions. Treatment options include a humeral head allograft, Remplissage, humeral rotation osteotomy, and hemiarthroplasty or total shoulder arthroplasty for older patients. When the lesion is greater than 40% of the articular surface Gerber et al. [15] suggest using an allograft technique in which a segment of the femoral head or other bone graft harvested from cadaveric donors could be used. In a similar manner, the procedure fittingly named Remplissage – meaning "to fill" –uses anchors and bone screws to fill the space with the infraspinatus tendon [16-18] as shown in **Figure 3**. Unfortunately, studies have shown that this procedure can reduce range of motion [19]. Rotational osteotomy shifts the surface defect posteriorly so that when the joint is rotated the defect will no longer engage with the glenoid [14]. Finally, hemi- or total- shoulder arthroplasty – replacement of the joint with artificial implants – while not incredibly common, is effective in a certain population of older patients [20].

The challenge that physicians face is determining which approach to use in which circumstance. Clearly there are factors such as the patient's age, level of activity, and additional

injuries that come into play but the author strongly believes that the physical characteristics of the lesion itself can also play a strong role in picking the best treatment for the patient.

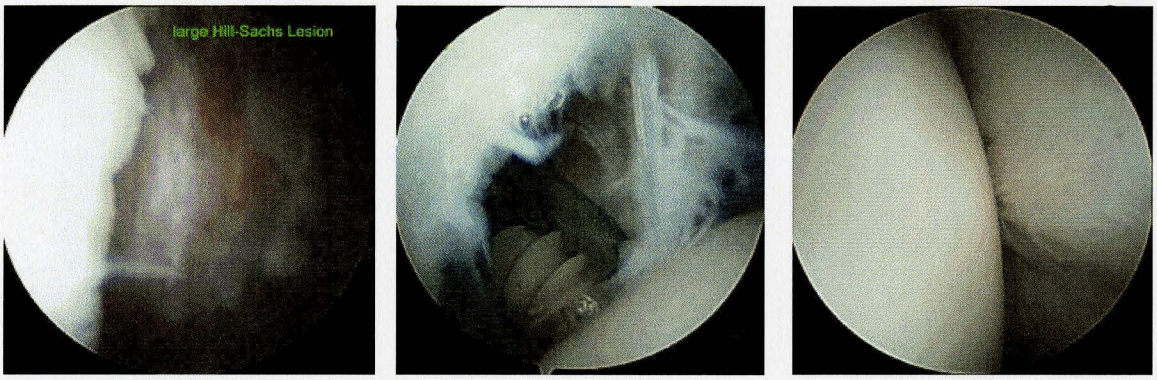

Figure 3. Remplissage procedure for HSL. *Left*: Arthroscopic image capture of HSL on humeral head. *Center*: Insertion of a large 5mm anchor. *Right*: Humeral head following Remplissage procedure. [17]

3.2 Methods

A review of glenohumeral instability literature was conducted specifically focusing on HSLs and analyses of their characteristics. The author summarized a number of sources in which the shape, location, and/or orientation of the lesion were discussed broadly in the larger context of repeat dislocations, surgical treatment, and surgical outcomes. From these data, a classification system was developed, to be applied when further work has been performed to quantify each parameter.

3.3 Results

3.3.1 Lesion Shape

In studies involving single cases or cadaveric models, authors were able to accurately measure the dimensions of the HSL [2, 11, 21]. For example, Yagishita and Thomas noted that the large degree of damage to their individual patient required them to switch from arthroscopic repair to open repair. At this time they were able to measure the lesion, 4 cm long by 2.5 cm wide by 2 cm deep [21]. Another study by Boileau et al. determined that a lesion greater than

25% of the articular head surface qualified as a large lesion [22]. Total articular surface area can be approximated using techniques developed to determine that average humeral head radius is 23 mm (range: 17-28 mm) [23].

A relatively large study of 42 patients carried out by Ungersbock et al. classified the lesions as mild, moderate, or severe based on length and depth [24]. While they did not identify a statistically significant trend between lesion size and redislocation rate, their data suggested that there were other factors at play for redislocation to be considered frequent. Unfortunately, they were unclear as to how these measurements were made, whether radiographically or physically during surgery. A modified version of the lesion size classification scheme developed by Ungersbock et al. has been adopted for this study (**Table 1**).

Table 1. HSL shape and size classification scheme.

	Depth (mm)	Length (mm)	Volume (mm^3)
Small	<2	<20	100
Medium	2-7	20-30	500
Large	>7	>30	2000

The width of the lesion is not being considered at this time, as the orientation of the lesion (engaging vs. non-engaging) is a larger determinant of redislocation rate.

3.3.2 Lesion Location

Radiologists are accustomed to looking at the level of the coracoid for signs of HSLs. However, in a stand-alone reconstruction of the humeral head, a new reference frame must be developed. It has been shown that anterior dislocations are most frequent and create a lesion on the posterior face of the articular surface that is likely to be engaging [6, 8, 20, 25]. To distinguish between the anterior and posterior surfaces of the humeral head, a coronal plane can be designated going through the largest protrusion of the greater tuberosity and the center of the

humerus. The center of the humeral head is offset 7 mm medially and 2 mm posteriorly relative to the humeral axis [23].

3.3.3 Lesion Orientation

As has been previously discussed, the difference in redislocation rate is highly dependent on whether the lesion is engaging or non-engaging. An engaging lesion is almost always an implication for required intervention [10, 16, 18, 26]. While the orientation of the lesion can be determined via purely qualitative methods, a unique approach can be taken to quantify this measurement. The HSL can be modeled in a simplified manner as an ellipsoid on the surface of a sphere. This ellipsoid would have two key dimensions, the long axis diameter and the short axis diameter. An axial plane going through the center of the humeral head can be modeled and the orientation of the lesion will be determined with the angle between the plane and the long axis diameter of the lesion. If the angle is between ±45°, the lesion will be characterized as engaging. Otherwise, it will be considered non-engaging. As far as we know, this is a novel approach to determining the orientation of the lesion so an extensive validation study will need to be carried out to determine which angles capture all engaging behavior.

3.4 Discussion

A critical geometry can be characterized as one with a large lesion that is oriented in an engaging manner. These qualities are seen most often on the posterior surface of the humeral head because anterior dislocations are most common. However, it is important to note than none of the traits are independent with respect to clinical outcomes. A patient with a large, non-engaging lesion may not experience continued glenohumeral instability while a small, engaging lesion may be quite severe.

With the most important HSL traits identified, future work can be carried out to computationally measure them. This will require integration of a 3D reconstruction techniques described below. While some preliminary strategies for characterizing the lesions have been suggested, future work will entail determining whether to work with the 3D structures as surfaces, a series of points, or as solid models.

4. Three-Dimensional Reconstruction of the Humeral Head

4.1 Introduction

Medical imaging techniques have provided physicians with the opportunity to make diagnoses and develop treatment plans for their patients noninvasively. However, there is always the need to reassess throughout the procedure, whether open or arthroscopic surgical techniques are being used. The advent of three-dimensional imaging has come with improved diagnosis and treatment planning. In the case of shoulder instability, having 3D humeral head reconstructions can allow decisions about whether special considerations should be made when performing a Bankart or Latarjet repair, especially if further study is able to alert physicians to critical HSL traits.

Magnetic Resonance Imaging (MRI), Computed Tomography (CT), and x-ray are commonly used to understand unexplained shoulder pain or survey damage following glenohumeral dislocation. When conventional methods are not adequate, a contrast agent may be injected to provide improved contrast between the target anatomy and surrounding anatomy. One example is magnetic resonance arthrography (MRA) – magnetic resonance imaging with the intra-articular injection of gadolinium contrast material. If acquired digitally, data from all of the aforementioned imaging modalities can be saved in DICOM (Digital Imaging and Communications in Medicine) format, which allows for computational analysis and processing of the data.

While contrast agents aid in highlighting the anatomical features of interest in a single image, there is often surrounding anatomy with similar traits that make it difficult to build 3D reconstructions. For this reason, image segmentation processes have been developed in which one can isolate a region of interest (ROI) within the data set. These techniques include Canny

edge detection, the Sobel technique, the level set method, and the active contours method. There are also commercial software packages available for 3D reconstruction of medical images; however, they can be costly, inefficient, and difficult to work with in further applications.

Important factors in selecting a 3D reconstruction technique for our application included a proven ability to work with complex medical images and a level of user control for further data processing. The technique chosen for this HSL study was developed in the Soft Tissue Biomechanics Laboratory at the University of Arizona [27, 28]. The segmentation process uses the active contours "snakes" method pioneered by Kass et al. [29] and further developed over two decades [27, 28, 30]. This methodology is appropriate for certain medical imaging applications because, even if initialized far from the ROI boundary, it can segment effectively. Another feature important for boundary detection is the ability to use image gradients rather than absolute pixel values [31, 32] The original purpose for creating this software was to build 3D reconstructions of abdominal aortic aneurysms (AAAs). The data sets were from CT scans with contrast. The snake protocol worked especially well in this case because the contrast agent set the blood vessel apart from surrounding structures.

In the case of the humeral head, this methodology can also be successful because medical images of this joint reveal distinguishable boundaries. The humeral head is composed of subchondral bone peripherally and cancellous bone centrally. While the variation in image intensities introduced some challenges, the anatomical properties of the bone provide a natural tool for boundary recognition.

4.2 Methods

The active contours method developed and described briefly above brings many strengths to the field of medical image reconstruction. However, there were some specific challenges associated

with processing the data from the humeral head scans available. While the contrast agent used for the AAA CT scans fills the vessel creating a sharp change in intensity between the artery and the surrounding tissue, contrast injected into the glenohumeral joint sometimes only partially surrounds the humeral head. This created unique obstacles for the image segmentation software, which were met with a data preprocessing technique in which the images were binarized. This and other methods employed in building 3D reconstructions of the humeral head are described in further detail below.

4.3.1 Snake Software

Segmentation of medical images requires insensitivity to convexities and concavities in the ROI. As was previously described, the selection of the active contours method was in line with the requirements for this and other requirements for medical image segmentation. For a complete theoretical description of the algorithm the reader is referred to previous publications [27, 28]. Briefly, within the ROI, the protocol requires the definition of an initial contour, known as the 'snake'. The contour defined by the user should meet one of the following two requirements: 1. it should entirely encapsulate the relevant geometry, or 2. it should lie entirely inside the relevant geometry. If considered in three dimensions, this initialized surface forms a volume that deforms to meet the boundaries of the geometry of interest. The volume is initialized as an icosahedron (20-sided polyhedron) with triangular element connectivity.

The volume is deformed according to the gradient vector field (GVF), an external force field acting on the snake to draw it towards the desired edge. The GVF and triangular mesh are defined by a set of 10 unitless parameters whose roles are defined in **Table 2**, whose behaviors can be physically interpreted as pressures, forces, etc. The goal of setting these parameters is to reach equilibrium between the internal and external forces at the boundary of the contour (as

shown in **Figure 4**). For example, too low of an α value would result in an overly compliant surface which would be dominated by the external force. Another example, a normal internal pressure applied on all surface points P_i, requires some thought because segments with low boundary gradients would allow the internal pressure to dominate over the GVF.

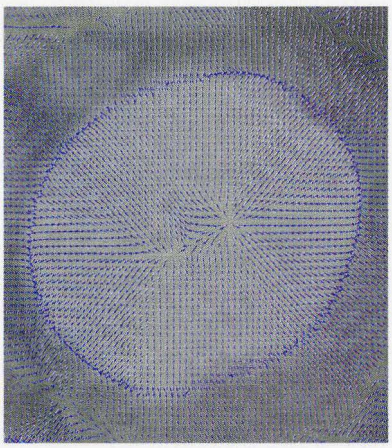

Figure 4. A typical GVF represented by a vector plot for a CT scan image. The boundary of the ROI of interest is clearly identifiable [27].

Table 2. Parameters for deformation of initial contour.

Snake Parameter	Definition	Default Value
α	Elastic stiffness of the deforming surface. Greater resistance to deformation in the normal direction with increasing α.	0.3
β	Bending stiffness of the snake. Smoother surface but less ability to conform to concavities with increasing β.	0.1
γ	Viscous behavior of the surface. Slower snake movement with increasing γ.	9
κ	Rigidity of the surface. GVF resistance with increasing κ.	3
P_i	Initial internal pressure of the contour. Faster deformation of the surface with increasing P_i.	2
d_{min}	Minimum length of triangle element leg. Decreased accuracy with increasing d_{min}.	2.1
d_{max}	Maximum length of triangle element leg. Decreased accuracy with increasing d_{max}.	4.3
σ	Standard deviation for GVF calculation. ROI size increase and blurring with increasing σ.	1
μ	Regularization parameter for image force weights and GVF. For data sets with noise, increasing accuracy with increasing μ.	10

As one might expect, having an understanding of the theoretical foundation of the snake software and having experience with the effects of each of the ten key parameters is critical to successfully building 3D reconstructions from medical images.

4.3.2 Raw Data

Two types of data were used in this study, one with MRA images of the humeral head from patients with HSLs and one with CT images of the humeral head from control Sawbones® models. The size of bone loss on the human glenoid is best visualized in the sagittal plane while HSL reconstructions are best done from axial slices.

Figure 5. A sampling of the Sawbones® models created for the validation stage of the study. *Left*: model #3 with a large, engaging HSL. *Center*: model #6 with a large, anterior HSL. *Right*: model #9 with a large, non-engaging HSL.

Table 3. Summary of control HSL data set models created.

	Engaging			Anterior			Non-Engaging		
Model #	1	2	3	4	5	6	7	8	9
Average Volume (cm^3)	0.1	0.6	2	0.1	0.5	2	0.1	0.4	1.9

The control data set was created from ten Sawbones® models (model 1051) of the humeral head, extending down a segment of the humeral shaft (**Figure 5**). The models are created from molds representing the anatomy of the human humerus. Model ten is representative of the intact humeral anatomy while each preceding model represents HSLs of varying size, position, and orientation. The traits of each model are summarized in . Overall, each of the key

lesion types, engaging, anterior, and non-engaging were represented by three models of varying size (typically approximately 0.1 cubic cm, 0.5 cubic cm, and 2 cubic cm).

The axial patient data sets were acquired as 2.0mm thick grayscale images 512×512 pixels in size, using the fast spoiled gradient-echo (FSPGR) method with contrast agent injection. Use of these de-identified patient data sets was approved by the University of Arizona Institutional Review Board under IRB00003012.

Each of the data sets were imported into DICOM viewer OsiriX to visualize the characteristics of the lesion in each slice and to determine how many slices to segment. Since the clinical data sets only included a few slices with the humeral shaft, all images were segmented. On the Sawbones® data sets that went 4-5cm down the humeral shaft, only the top-most part of the shaft was segmented.

4.3.3 Data Binarization

As can be seen from images from a single patient (**Figure 6**), there can be regions within the humeral head with high intensity and regions with low intensity. This is often due to the transition from cortical to trabecular moving inwards towards the center of the humeral head. We can also see that, while a contrast agent is present, bright signal does not always help to create a uniform boundary around the entire region of interest.

To improve segmentation in the active contours algorithm, preprocessing was done on the images to render them black and white based on the range of intensities within the geometry of interest. Once the image data was binary it was imported to continue processing as usual.

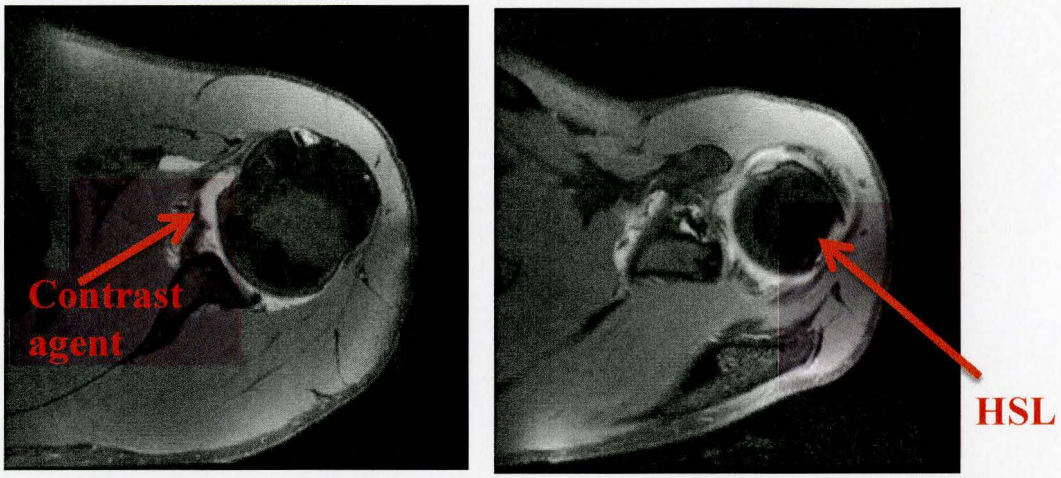

Figure 6. An inferior (left) and superior (right) slice from a patient data set.

4.3.4 Determining Optimal Parameters

The optimal values for the ten snake parameters were determined experimentally by the author using the decision scheme shown in **Figure 7**. The first key step is to determine whether there is wide ranging ROI intensity between the various image in a series. If this is the case, binarizing the data is recommended. The spacing must be set so that the resolution is the same in the x-, y-, and z-directions. In the z-direction, image data will be interpolated from the original data set. If there are discontinuities or image artifacts within the ROI, applying a blur effect can help to eliminate the problem. Blurring takes the average and standard deviations of surrounding pixels and applies it to the edges of the ROI. To initialize the contour, the center of the ROI should be selected. The desired radius should either be completely inside or completely outside the ROI, but as close to the boundary as possible. Determining whether the contour is satisfactory is purely a qualitative decision. The contour will slowly begin to take the shape of the humeral head with each iteration of snake and GVF parameters. If the contour is satisfactory, the data – including surface points and information about the triangular mesh connectivity – should be saved.

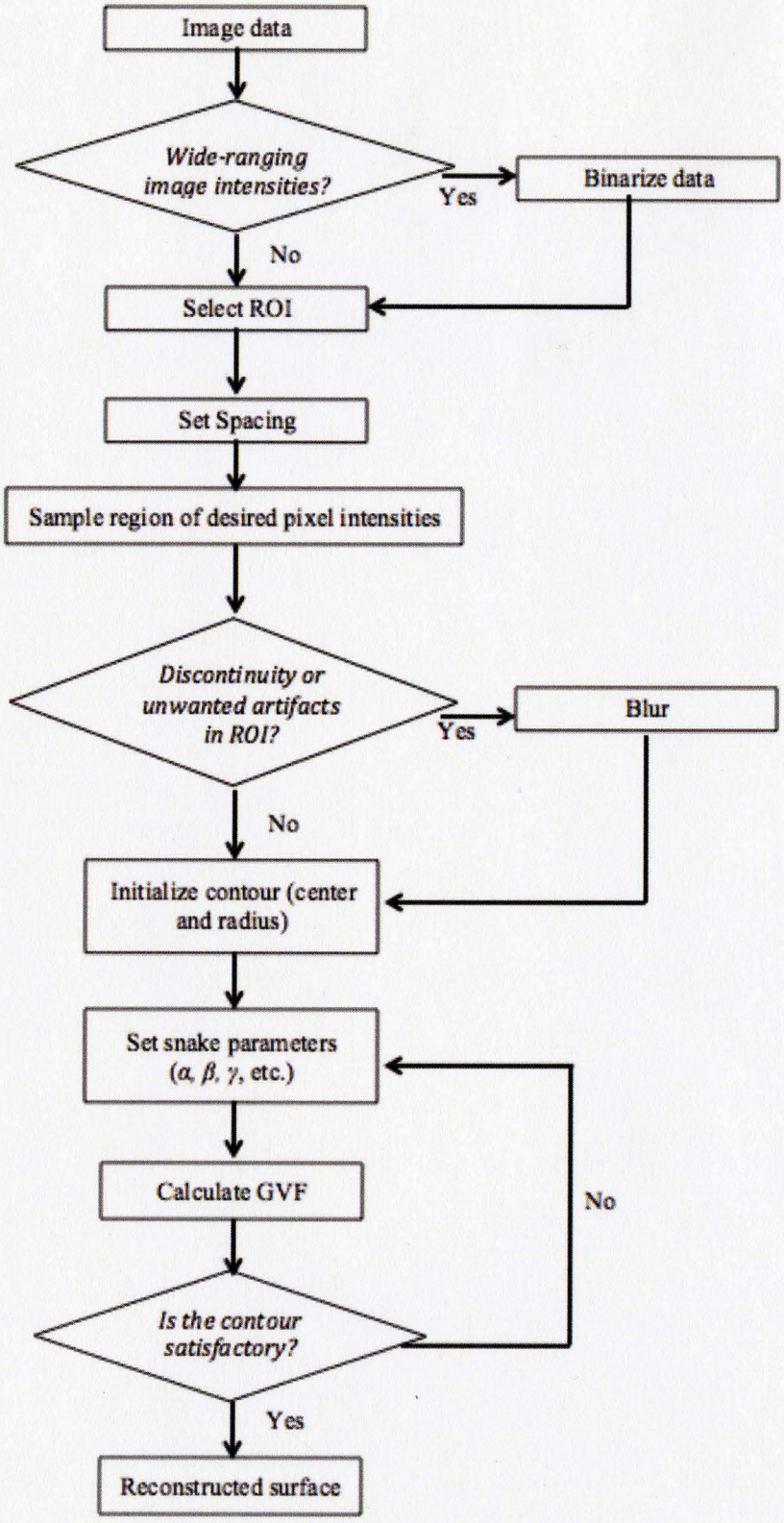

Figure 7. Flowchart of 3D reconstruction algorithm.

4.3 Results

According to **Figure 7**, a trial and error approach was taken to optimize the 3D reconstruction. The final reconstruction was approved based on visual inspection. Trends were observed as the author became more and more familiar with the effects of each parameter. Eventually, results such as those shown in **Figure 8** were achieved. The parameter values used for various reconstructions toward reaching this goal are highlighted in Appendix 1.

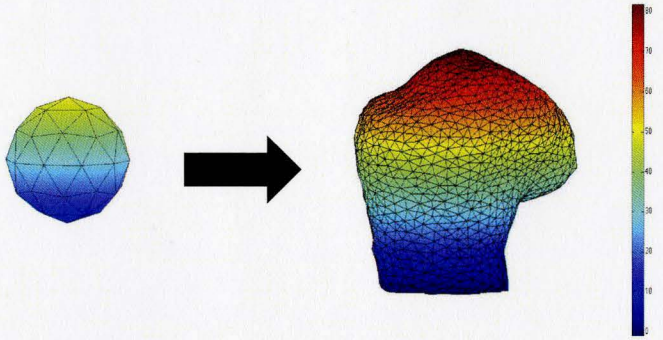

Figure 8. Example of a successful 3D reconstruction. *Left:* Initial contour from which 3D reconstruction was built. *Right:* Final contour representing 3D reconstruction from which one can see the bicipital groove (physiological) and the Hill-Sachs Lesion (pathological). Colormap represent height in mm.

Briefly, one can see in results for Patients 3 and 4, that understanding the contributions of α and γ was critical. When the GVF did not provide a completely defined ROI boundary, it was important to increase the values of these parameters to slow the snake by making it more stiff and viscous. This way the user has more control in between deformation stages to make sure the contour does not "leak out" of the surface boundary.

4.4 Discussion

For this first stage toward characterizing HSLs, an active contours snake method was used to reconstruct 3D surfaces from the medical images provided. Key points of this process include being aware of the effect of each snake parameter and binarizing the data when

necessary to provide more contrast and clearer boundaries. While the ability to select the ROI and control the snake parameters is advantageous in many respects, the disadvantage is that there can be widespread variability in results between users. Minimizing this variability is something to work towards in the future. This can be accomplished by having numerical measures to help make the decisions at each step in the reconstruction algorithm.

Further work in improving the accuracy of the 3D reconstructions can be to improve the binarization scheme where the ROI is all only one intensity. This would likely require some image processing expertise to detect the region boundaries and fill the space within the boundaries. In addition to improving pre-processing, while the snake is deforming one can visualize the snake boundary with respect to each slice of the original MRA scan. This would likely help to further understand how the parameters play a role in the reconstruction. Finally, a post-processing routine to smooth the final surface, might also help to improve the final product.

5. Conclusions

The goal of this study was to characterize the traits of HSLs and build 3D reconstructions of the humeral head from HSL patient scans. This is important because the characteristics of the lesion can play a crucial role in the success of bony repairs in patients with glenohumeral instability. An active contour segmentation algorithm was employed towards the goal of further studying the role of HSLs in contributing to clinical outcomes. The medical imaging modalities, MRA and CT in this case, must provide a sufficient intensity gradient for the segmentation protocol to yield geometries with appreciable accuracy. The benefit of creating reconstructions of the humeral head is the ability to visualize the HSL defect in 3D space. More importantly, this sets the stage for future work in quantifying the characteristics of the lesion, namely shape, location, and orientation.

The ability to qualitatively and quantitatively examine geometries using processing of medical images is critical. In addition to allowing characterization of traits that today are believed to play a role in surgical outcomes, future analyses could shed light on critical stress concentrations as a result of altered geometry. This study will have far reaching implications in the future, both in carrying on with HSL studies and reconstructing other critical anatomy in the human body.

6. Appendix

Patient 1:

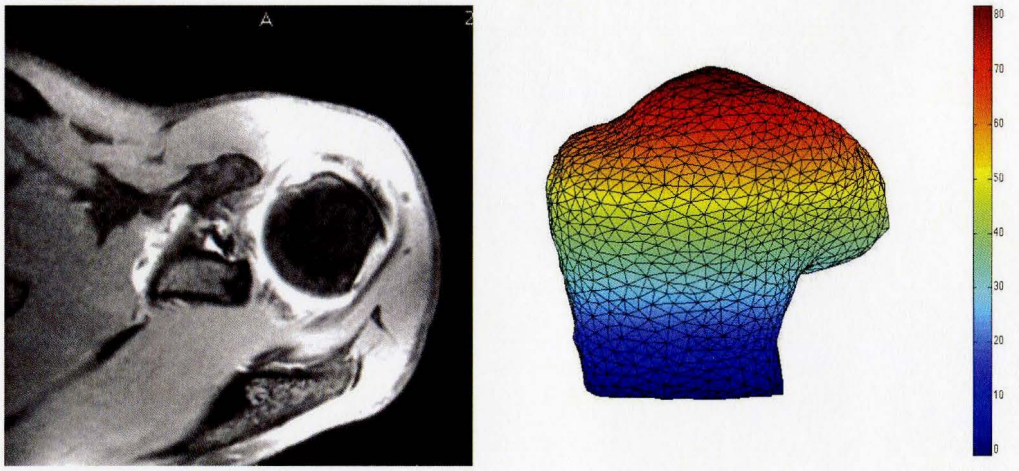

Figure 9. Raw data and results for Patient 1.

Table 4. Parameter values used for Patient 1 3D reconstruction.

Snake Parameter	Initial Value (1-20)	(21-40)	(41-60)	(61-80)	(81-100)	(101-120)	(101-120)
α	0.30	0.30	0.35	0.35	0.35	0.35	0.35
β	0.10	0.10	0.10	0.10	0.15	0.15	0.15
γ	9	9	11	11	11	11	11
κ	3	3	3	3	3	3	3
P_i	2	2	2	2	2	2	2
d_{min}	2.1	2.1	2.1	2.1	2.5	3.0	3.0
d_{max}	4.3	4.3	4.3	4.3	4.3	4.3	4.3
σ	1	1	1	1	1	1	1
μ	11	11	11	11	11	11	11

Patient 3:

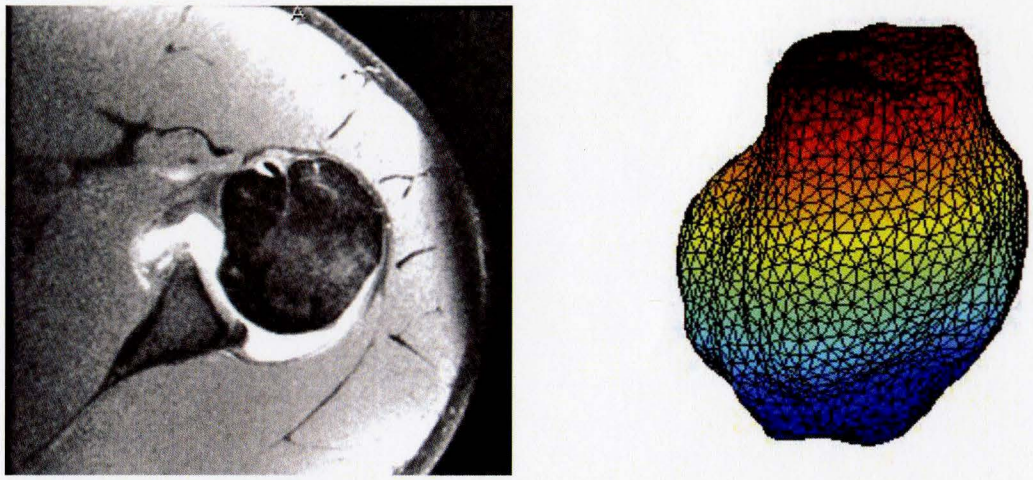

Figure 10. Raw data and results for Patient 3.

Table 5. Parameter values used for Patient 3 3D reconstruction.

Snake Parameter	Initial Value (1-20)	(21-40)	(41-60)	(61-80)	(81-100)	(101-120)	(101-120)
α	0.35	0.35	0.35	0.35	0.35	0.35	0.35
β	0.10	0.10	0.10	0.10	0.10	0.10	0.10
γ	11	11	11	11	11	11	11
κ	3	3	3	3	3	3	3
P_i	2	2	2	2	2	2	2
d_{min}	2.1	2.1	2.1	2.1	2.1	2.1	2.1
d_{max}	4.3	4.3	4.3	4.3	4.3	4.3	4.3
σ	1	1	1	1	1	1	1
μ	10	10	10	10	10	10	10

Patient 4:

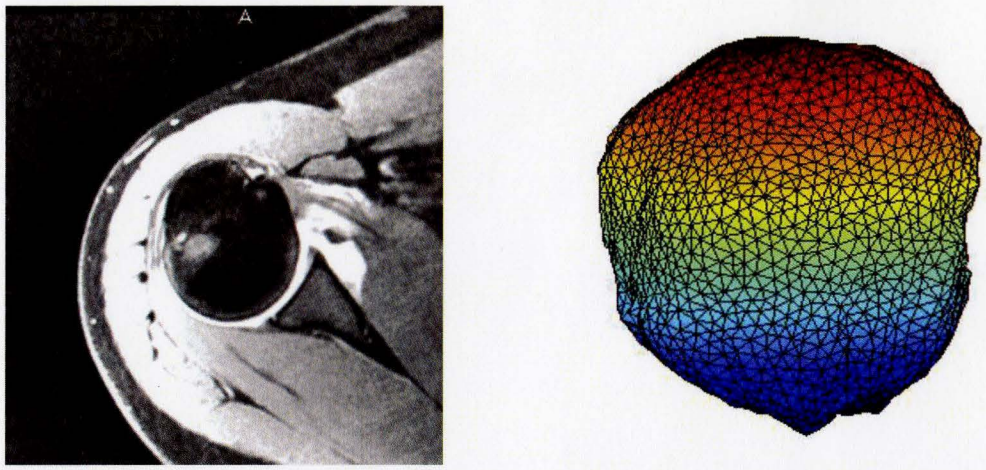

Figure 11. Raw data and results for Patient 4.

Table 6. Parameter values used for Patient 4 3D reconstruction.

Snake Parameter	Initial Value (1-20)	(21-40)	(41-60)	(61-80)	(81-100)	(101-120)	(101-120)
α	0.30	0.30	0.35	0.35	0.35	0.35	0.35
β	0.10	0.10	0.10	0.10	0.10	0.10	0.10
γ	9	9	11	11	11	11	11
κ	3	3	3	3	3	3	3
P_i	2	2	2	2	2	2	2
d_{min}	2.1	2.1	2.1	2.1	2.1	2.1	2.1
d_{max}	4.3	4.3	4.3	4.3	4.3	4.3	4.3
σ	1	1	1	1	1	1	1
μ	10	10	10	10	10	10	10

7. References

1. Matsen FA, Thomas SC, Rockwood CA., *The Shoulder*. 1990, Philadelphia: WB Saunders Co.
2. Blasier RB, Guldberg RE, Rothman ED. Anterior shoulder stability: Contributions to rotator cuff forces and the capsular ligaments in a cadaver model. *J Shoulder Elbow Surg*, 1992(1): p. 140-150.
3. Dodson CC, Cordasco FA. Anterior glendohumeral joint dislocations. *Orthop Clin North Am*, 2008(4): p. 507-518.
4. Hovelius L, Augustini BG, Fredin H, et al. Primary anterior dislocation of the shoulder in young patients. A ten-year prospective study. *J Bone Joint Surg Am*, 1996(11): p. 1677-1684.
5. Baker CL. Intraarticular pathology in acute, first-time anterior shoulder dislocation: An arthroscopic study. *Arthroscopy*, 1994(10): p. 478-479.
6. Calandra JJ, Baker CL, Uribe J. The incidence of Hill-Sachs lesions in initial anterior shoulder dislocations. *Arthroscopy*, 1989(5): p. 254-257.
7. Norlin R. Intraarticular pathology in acute, first-time anterior shoulder dislocation: An arthroscopic study. *Arthroscopy*, 1993(9): p. 546-549.
8. Taylor DC, Arciero RA. Pathologic changes associated with shoulder dislocations. Arthroscopic and physical examination findings in first- time, traumatic anterior dislocations. *Am J Sports Med*, 1997(25): p. 306-311.
9. Edwards TB, Boulahia A, Walch G. Radiographic Analysis of Bone Defects in Chronic Anterior Shoulder Instability. *Arthroscopy: The Journal of Arthroscopic and Related Surgery*, 2003(7): p. 732-739.
10. Burkhart SS, De Beer JF. Traumatic Glenohumeral Bone Defects and Their Relationship to Failure of Arthroscopic Bankart Repairs: Significance of the Inverted-Pear Glenoid and the Humeral Engaging Hill-Sachs Lesion. *Arthroscopy: The Journal of Arthroscopic and Related Surgery*, 2000(7): p. 677-694.
11. Itoi E, Lee SB, Berglund LJ, et al. The effect of a glenoid defect on anteroinferior stability of the shoulder after Bankart repair: A cadaveric study. *J Bone Joint Surg*, 2000(82A): p. 35-46.
12. Itoi E, Lee SB, Amrami, KK, Wenger DE, An KN. Quantitative Assessment of Classic Anteroinferior Bony Bankart Lesions by Radiography and Computed Tomography. *Am J Sports Med*, 2003(1): p. 112-118.
13. Lo I, Parten PM, Burkhart SS. The Inverted Pear Glenoid: An Indicator of Significant Glenoid Bone Loss. *Arthroscopy: The Journal of Arthroscopic and Related Surgery*, 2004(2): p. 169-174.
14. Weber B, Simpson LA, Hardegger F, Gallen S. Rotational humeral osteotomy for recurrent anterior dislocation of the shoulder associated with a large Hill-Sachs lesion. *J Bone Joint Surg*, 1984(9): p. 1443-1450.
15. Gerber C, Lambert SM. Allograft Reconstruction of Segmental Defects of the Humeral Head for the Treatment of Chronic Locked Posterior Dislocation of the Shoulder. *J Bone Joint Surg*, 1996(3): p. 376-382.

16. Purchase R, Wolf EM, Hobgood ER, et al. Hill-Sachs "Remplissage": An Arthroscopic Solution for the Engaging Hill-Sachs Lesion. *Arthroscopy: The Journal of Arthroscopic and Related Surgery*, 2008(6): p. 723-726.
17. Shah N, Funk L. Remplissage Procedure. *Shoulderdoc*, 2011.
18. Koo S, Burkhart SS, Ochoa E. Arthroscopic Double-Pulley Remplissage Technique for Engaging Hill-Sachs Lesions in Anterior Shoulder Instability Repairs. *Arthroscopy: The Journal of Arthroscopic and Related Surgery*, 2009(11): p. 1343-1348.
19. Deutsch A, Kroll DG. Decreased range of motion following arthroscopic remplissage. *Orthopedics*, 2008(5): p. 492.
20. Flatow E, Miller SR, Neer CS. Chronic anterior dislocation of the shoulder. *J Shoulder Elbow Surg*, 1993(1): p. 2-10.
21. Yagishita K, Thomas BJ. Use of allograft for large Hill-Sachs lesion associated with anterior glenohumeral dislocation: A case report. *Injury, Int J Care Injured*, 2002(33): p. 791-794.
22. Boileau P, Villalba M, Hery JY, et al. Risk Factors for Recurrence of Shoulder Instability After Arthroscopic Bankart Repair. *J Bone Joint Surg*, 2006(8): p. 1755-1763.
23. Robertson D, Yuam J, Bigliani LU, Flatow EL, Yamaguchi K. Three-Dimensional Analysis of the Proximal Part of the Humerus: Relevance to Arthroplasty. *J Bone Joint Surg*, 2000(11): p. 1594-1602.
24. Ungersbock A, Michel M, Hertel R. Factors influencing the results of a modified Bankart procedure. *J Shoulder Elbow Surg*, 1995(5): p. 365-369.
25. Kim D, Yoon YS, Yi CH. Prevalence Comparison of Accompanying Lesions Between Primary and Recurrent Anterior Dislocation in the Shoulder. *Am J Sports Med*, 2010(10): p. 2071-2076.
26. Bushnell B, Creighton A, Herring MM. Hybrid Treatment of Engaging Hill-Sachs Lesions: Arthroscopic Capsulolabral Repair and Limited Posterior Approach for Bone Grafting. *Techniques in Shoulder & Elbow Surgery*, 2007(4): p. 194-203.
27. Ayyalasomayajula A. Porohyperelastic Finite Element Modeling and 3D Reconstruction of Abdominal Aortic Aneurysms. *Thesis,* 2008, University of Arizona: Tucson.
28. Ayyalasomayajula A, Polk A, Basudhar A, et al. Three Dimensional Active Contours for the Reconstruction of Abdominal Aortic Aneurysms. *Annals of Biomedical Engineering*, 2010(1): p. 164-176.
29. Kass M, Witkin A, Terzopoulos D. Snakes: Active Contour Models. *International Journal of Computer Vision*, 1988: p. 321-331.
30. Xu C, Prince JL. Snakes, Shapes, and Gradient Vector Flow. *IEEE Transactions on Image Processing*, 1998(3): p. 359-369.
31. Peng J, Li Q, Kuo JC, Zhou M. Estimating gaussian curvatures from 3D meshes. *Human Vision and Electronic Imaging VIII, Proceedings of the SPIE*, 2003.
32. Xu C, Prince JL. Gradient vector flow: a new external force for snakes. *IEEE Proc. Conference on Computers and Visual Pattern Recognition*, 1997.